ELSEVIER

Contents lists available at ScienceDirect

Wear

journal homepage: www.elsevier.com/locate/wear





Surface engineering strategies for aerospace composite repairs: Machining and texturation of additive manufacturing parts by abrasive waterjet

Arjun Chandra Shekar a,b, Jean-Philippe Leclair, Redouane Zitoune b,c,*, Lucas A. Hof a,**

- a Department of Mechanical Engineering, École de technologie supérieure, 1100 rue Notre-Dame Ouest, Montréal, Québec, H3C1K3, Canada
- b Institut Clément Ader (ICA), Université de Toulouse, CNRS, INSA, ISAE-SUPAERO, Mines-Albi, UPS, 3 Rue Caroline Aigle, 31400, Toulouse, France
- ^c CINTRA CNRS/NTU/THALES, IRL 3288, Research Techno Plaza, 637553, Singapore

ARTICLE INFO

Keywords: Carbon/thermoplastic composites Additive manufacturing Abrasive waterjet process Composite repair Surface texturation

ABSTRACT

In aerospace maintenance, repair and overhaul operations, additive manufacturing (AM) holds great potential for composite repair, providing a precise and customized approach to fabricating repair patches for damaged structures and reduce waste. Given the circularity and economic advantages, repairing composite structures is often preferable to replacement. This study explores the use of abrasive waterjet process for machining and texturing AM composites composed of micro carbon infused nylon matrix and continuous carbon fiber reinforcement. Four surface conditions were investigated: (I) machined without additional surface preparation, and (II, III, IV) machined followed by three levels of texturation - good, medium, and poor. These surfaces are quantitatively evaluated based on crater volume (Cv) and arithmetic mean height (Sa). The mechanism of material removal was investigated by surface texture analysis and scanning electron microscopy. A prediction model was developed and experimentally validated for assessing the correlation of Cv and Sa. Results show an ascending trend in both Cv and Sa values from condition I to IV. The study reveals important findings on machined surface characteristics and their preparation for adhesive bonding, which are crucial for integrating repair patches onto parent structures.

1. Introduction

Defects

Modern industrial scenarios demand emphasis on sustainability and resource optimization [1] driving advancements in circular manufacturing practices [2,3]. In aerospace engineering, 'repairing' structures rather than 'replacing' them has emerged as a key strategy, driven by both sustainability and cost-efficiency considerations [4]. Additive manufacturing (AM) plays a significant role in formulating precise and customizable solutions within the realm of Industry 4.0/5.0 [5] and could integrate well into maintenance, repair and overhaul operations. Material extrusion (MEX), one of several AM techniques [6], in which the filament is heated and deposited layer by layer through a controlled extrusion process, has recently gained significant attention due to the development of long fiber-reinforced filaments [7]. The orientation of these fibers, governed by the filament deposit direction,

plays an important role in achieving strong mechanical properties of the printed parts.

Designed to provide superior strength-to-weight ratios, excellent fatigue resistance, and robust corrosion resistance, CFRP composites are ideal for a variety of aerospace applications [8–10]. Nevertheless, during service, CFRP composites are susceptible for various forms of structural damage from impact and erosion. This damage can lead to loss of load-bearing capabilities, reduced fatigue life, and compromised aircraft integrity [11]. When an aircraft is stationed for repair, it is essential to follow agile procedures that restore the mechanical properties of the repaired area to closely match those of the undamaged structure. Repair procedures are generally broken down into six phases:

1) identifying and characterizing the damage zone; 2) machining of damaged area; 3) surface preparation for repair; 4) designing a patch to match the machined dimensions; 5) adhesive bonding; and finally, 6)

E-mail addresses: arjun-chandra-shekar.chintalapalli.1@ens.etsmtl.ca (A. Chandra Shekar), jean-philippe.leclair.1@ens.etsmtl.ca (J.-P. Leclair), redouane. zitoune@iut-tlse3.fr (R. Zitoune), lucas.hof@etsmtl.ca (L.A. Hof).

This article is part of a special issue entitled: WOM2025 published in Wear.

^{*} Corresponding author. Institut Clément Ader (ICA), Université de Toulouse, CNRS, INSA, ISAE-SUPAERO, Mines-Albi, UPS, 3 Rue Caroline Aigle, 31400 Toulouse, France 3CINTRA CNRS/NTU/THALES, IRL 3288, Research Techno Plaza, 637553, Singapore.

^{**} Corresponding author.

inspection and certification [11]. In this context, machining of the damaged area (phase 2) is typically carried out using traditional machining processes (e.g. milling, grinding and trimming) [8]. However, these processes are disadvantageous and unsuitable for CFRP composites due to the mechanical and thermal damage they can induce [12,13]. The complexity of machining CFRP composites arises from the variations in thermal, mechanical and physical material properties between the fiber reinforcements and the polymer matrix. Additionally, the mechanisms of material removal is highly influenced by the cutting speed and fiber orientation [14]. Also, it poses a health risk to operators, as they unavoidably tend to inhale the noxious fine particles generated by the intricate cutting mechanisms during machining [15]. Moreover, the deviations in the mechanical behavior of composites from their original bulk properties are often attributed to the quality of the machining process [16–18].

Abrasive waterjet (AWJ) process is a well-regarded non-traditional material removal technique, recognized for its efficiency across a wide spectrum of materials, including CFRP composites [19]. AWJ has been increasingly employed in the material removal of composites, and several studies also confirm its feasibility [20-22]. Prior research has demonstrated the effectiveness of AWJ in enhancing the surface quality of fiber-reinforced polymers through the optimization of machining variables for carbon/epoxy composites [12,16,23]. Unlike traditional methods, AWJ exerts minimal forces on the workpiece during machining and eliminates the need for specialized tooling, thereby preventing the formation of heat affected zones [9]. In AWJ machining, the material removal occurs through micro-erosion resulting from the impact of abrasive particles. These particles strike the workpiece surface, inducing high contact stresses leading to micro fractures, chipping and lateral crack formation [24]. In the case of carbon/epoxy composites, this process results in broken fibers and micro-craters on the machined surface due to the brittle nature of the reinforced carbon fiber (CF), resulting in a combination of micro-machining and brittle fracture [8,25,26]. Haddad et al., showed that carbon/epoxy specimens trimmed using the AWJ process exhibited compressive failure stress at values 15 % higher than those trimmed with conventional methods such as burr tools [23]. However, literature lacks comprehensive studies on the machining and texturing quality achieved through AWJ processes and their impact on the mechanical behavior of composite structures made from carbon/thermoplastic composites. These insights are crucial in the field of composite repair. To the best of our knowledge, the mechanisms of material removal in AM based carbon/thermoplastic composite materials during AWJ process have not yet been identified.

Surface roughness, Ra, the line-based measurement technique is commonly used to evaluate the machined surfaces. However, its application to composite materials made form carbon/epoxy has produced inconsistent results [23,27,28]. Research suggests that surface roughness may not be a clear indicator of strength in polymer composites, with delamination being a more critical factor [29]. Therefore, while Ra is a well-suited parameter for assessing surface roughness in metals [30], it may not reliably characterize machined composite structures. Relying solely on Ra to assess machining quality may not capture the full scope of surface characteristics [8,27]. Hence, crater volume (Cv) is increasingly recognized as a preferred criterion for surface quality evaluation during machining of composite materials [8,9,11]. Cv, quantifies the volume of material removal per unit area due to the impact of AWJ machining. It can be defined mathematically as:

$$Cv = \frac{\int h(x,y)dA}{A}$$
 (1)

Where: A is the area over which the crater is formed (in cm^2) and h (x, y) is the depth of the crater at any point (x, y) on the surface (mm). The equation calculates the total area of the crater (in mm^3) and then normalizes it by the area (in cm^2) to provide the crater volume per unit area. Unlike Ra, Cv provides a deeper assessment of surface integrity,

particularly in carbon/epoxy composites and correlates well with mechanical behavior, making it pertinent over the traditional roughness metrics [8,9,31]. Sa, the arithmetic mean height of a surface, complements Cv by assessing the average height deviations and surface roughness [11,13]. Together, Cv and Sa offer a comprehensive evaluation, capturing both the volumetric and roughness aspects. Applying these parameters to carbon/thermoplastic composites shows promise for better understanding surface characteristics.

As outlined in Fig. 1, this study investigates the integration of AWJ machining and continuous fiber MEX fabrication for composite repair. By evaluating various surface texturation intensities and identifying optimal AWJ parameters, this research seeks to enhance adhesive bonding and repair effectiveness in MEX fabricated parts. The experimental approach involves creating four distinct surface conditions based on texturation intensity. These conditions are assessed using surface topography analysis, as well as Scanning Electron Microscopy (SEM) characterization. The study investigates unidirectional (UD) and multidirectional (MD) configurations. Additionally, this work involves the development of a prediction model to assess key surface characteristics, specifically Cv and Sa, offering a quantitative framework for predicting outcomes in the context of composite repair.

2. Materials and experimentation

2.1. Composite materials

This study employs a Markforged Mark-Two 3D printer, which integrates MEX with continuous filament fabrication techniques. Specimens were fabricated using continuous CF reinforcement within an onyx thermoplastic matrix, both sourced from Markforged Corporation. *Onyx*, a commercial term coined by Markforged, refers to a micro CF filled nylon filament known for its high strength, toughness, and excellent surface finish [32]. The continuous carbon fibers tows consist of several individual carbon fibers strands that are encased in an onyx thermoplastic matrix. The fibers as well as the matrix are sizing compatible. Appropriate spacing in the range of 200–250 μm was achieved between fiber tows in the continuous fiber samples. During the MEX process, this thermoplastic coating thermally fuses to the part as it is extruded through the heated nozzle. The mechanical properties of the composite used in this study are listed in Table 1 [33].

Print settings were configured using the proprietary software Eiger™, utilizing a 100 % infill strategy with an isotropic fiber fill type to ensure uniform material properties, structural integrity and suitability for subsequent machining and texturing operations. The 100 % infill strategy reduces internal voids and porosity, resulting in dense specimens with minimized internal voids and porosity, critical for maintaining mechanical performance against the forces exerted during AWJ machining. The isotropic fiber type provides consistent mechanical properties across all in-plane directions, especially under interlaminar loading, which is essential for accurately evaluating surface characteristics during AWJ machining. The printer features a dual-nozzle system: one dedicated to the matrix and the other to the reinforcement. The matrix and fiber nozzles operate at 272 °C and 250 °C respectively, with the fiber nozzle alternating with the matrix nozzle, embedding continuous CF within the matrix layers. The onyx deposition is synchronized with the print head movement to ensure alignment with the design strategy. Only one nozzle extrudes material at a time, with each layer being 0.125 mm thick. The non-heated, kinematic coupled build platform allows for immediate part removal upon print completion. Fig. 2 provides the working principle schematic, the printing process of the plate, and an illustration of the stacking sequence for both orientations. As detailed in Table 2, these dimensions were selected to utilize the maximum printable area and produce the largest possible individual specimens of 100 mm \times 25 mm from each plate. An additional margin around the edges was included to ensure uniformity in specimen profiles, allowing for precise cutting. This margin also accounted for the CF

Fig. 1. Overview of the research methodology used in this study.

Table 1
Mechanical properties of onyx and continuous carbon fiber used in this work (adapted from Ref. [33]).

Parameter	Onyx	Carbon Fiber
Tensile strength (MPa)	-	800
Tensile modulus (GPa)	2.4	60
Tensile strain at break (%)	25	1.5
Flexural strength (MPa)	71	540
Flexural modulus (GPa)	3.0	51
Flexural strain at break (%)	-	1.2
Compressive strength (MPa)	-	420
Compressive modulus (GPa)	-	62
Compressive strain at break (%)	-	0.7
Izod Impact – notched (J/m)	330	960

layer cuts at the plate ends, ensuring that only the highest quality sections were selected for the study. The thicknesses of 2.28 mm and 2.5 mm were chosen to closely replicate typical aircraft fuselage frames, which generally range from 2 mm to 3 mm [34–36].

A specific 25 mm \times 25 mm area on the surface of each 100 mm \times 25 mm specimen was designated for machining and texturation. The onyx-CF composite achieved an estimated fiber volume fraction of 56 %, calculated using the rule of mixtures based on the cross-sectional areas of both CF and the matrix, assuming uniform thickness [37].

2.2. Machining and texturing using AWJ

The cutting, machining and texturing of specimens were carried out

using an AWJ machine, equipped with a Hyplex pump and Paser 4 nozzle called Mach 4c from Flow International corporation. The AWJ process parameters are provided in Table 3. The machining parameters considered in this work were obtained through a systematic approach, combining insights from earlier literature on texturing and refined through iterative experimental trials [11,38]. Previous research highlights WP and TS as the most influential parameters in AWJ processes for material removal [8,9]. For texturing, earlier studies identified optimal ranges of WP (60-100 MPa) and TS (10-15 m/min) to balance material removal efficiency and surface integrity [39]. Drawing from these findings, a WP of 100 MPa was identified as optimal for machining, ensuring effective material removal while preserving the structural stability of the composite specimens, as higher pressures risked compromising the specimens. With WP fixed at 100 MPa, TS was optimized through iterative trials, leading to the selection of 5 m/min as the optimal speed for machining. This parameter combination, as detailed in Table 3, produced clean, defect-free cuts ensuring that the specimens were well-prepared for subsequent texturing and analysis.

Abrasives used in the operations were procured from Wuxi Ding Long Minerals Ltd. To ensure stability during machining, the MEX – fabricated composite specimens were securely fastened to a long wooden platform attached to the machining table, preventing any inadvertent movement caused due to waterjet's traverse between passes. A raster scan pattern strategy is employed along the y-direction, as illustrated in Fig. 3a. To mitigate excessive material erosion caused by variations in traverse speed occurring due to jet direction changes, a 100 mm jet traverse extension was added on both sides of the specimen [11]. This extension helps counteract changes in the machine head induced when the jet

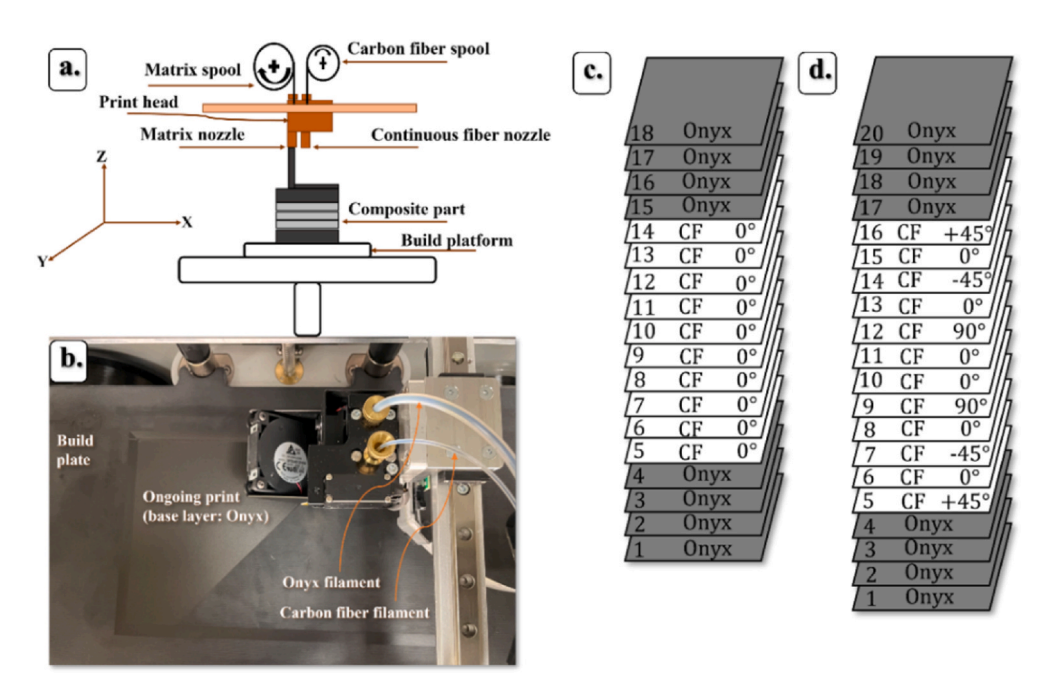


Fig. 2. MEX fabricated composite used in this study: a) Schematic of the printing process, b) plate during print, c) and d) Illustration of stacking sequence for UD and MD orientation respectively.

Table 2
Specimen dimensions and printing details.

Parameter	Details
Plate dimensions - UD (mm)	210 x 120 x 2.28
Plate dimensions - MD (mm)	210 x 120 x 2.5
Individual specimen dimensions (mm)	100 x 25
Infill strategy	Solid, 100 % density
Print orientation (UD)	First and last 4 layers: Onyx thermoplastic, central layers: Carbon fiber oriented at 0°
Print orientation (MD)	First and last 4 layers: Onyx thermoplastic, central layers: Carbon fiber oriented at $(+45^{\circ}/0^{\circ}/-45^{\circ}/0^{\circ}/90^{\circ})$ s

Table 3 Abrasive waterjet machining and texturation parameters.

	Value	Cutting	Machining	Texturation
Fixed Parameters				
Mixing tube diameter, mm	1.016	-	_	_
Mixing tube length, mm	76	_	_	_
Nozzle diameter, mm	0.3302	_	_	_
Nature of abrasive	Garnet	-	_	_
Abrasive grit number, #	120	-	_	_
Abrasive flow rate, Kg/min	0.34	-	_	_
Variable Parameters				
Waterjet pressure, MPa (P)	-	150	100	80/85/100
Jet traverse speed, m/min (TS)	-	5	5	10//15
Scan step, mm (SS)	-	1	1	1
Stand-off distance, mm (SoD)	-	3	100	100

reverses direction between passes. A scan step of 1 mm and a stand-off distance of 100 mm were maintained throughout machining and texturing to ensure uniformity and reduce abrasive embedment contamination [9,10,39]. While specific tests for scan step and stand-off distance were not conducted in this work, the values of 1 mm and 100 mm respectively have been validated in earlier research [9,39], which demonstrated their effectiveness in achieving consistent results and minimizing contamination.

The composite specimens were cut from the parent plate using the parameters in Table 3, resulting in clean, defect-free cuts with no delamination or matrix bulging. This ensured the integrity of the specimen edges for subsequent machining and texturing processes (Table 4). After cutting, the specimens were machined to remove approximately half their material thickness in preparation for texturing. Preliminary tests identified a waterjet pressure of 100 MPa as optimal for precise material removal and consistent surface profiles, as shown in Fig. 3b.

After completing the machining phase (Condition I), the objective shifted to assessing the impact of machining parameters on texturation quality (conditions II – IV). In this regard, a series of systematic trials were conducted to identify optimal input parameters for fine texturation without significantly reducing specimen thickness. Waterjet pressures ranging from 80 to 100 MPa were tested in 5 MPa increments, while jet traverse speeds were varied between 5 and 15 m/min [39]. This range of waterjet pressures (80–100 MPa) was established based on insights from our earlier work [39], which investigated surface texturing parameters for AM composites, and identified this range as optimal for effective material removal. These insights were considered in the current study to test pressures within this range at 5 MPa increments to texture the machined specimens.

After each trial, surface profilometric studies were conducted to evaluate material removal depth and surface quality in relation to the input variables. As a result, these trials yielded three distinct texturing conditions: 80 MPa at 10 m/min (condition II), 85 MPa at 10 m/min (condition IV), showing a progressive deterioration in surface quality without compromising

structural integrity (Fig. 3b). The distinction between 'machined' and 'textured' surfaces was established through a combination of thickness measurements and quantitative evaluation of crater volume (Cv) and arithmetic mean height (Sa) obtained through surface profilometric measurements. Indeed, in texturation only a thin layer of material is removed, while machining refers to more significant material removal. It should be noted that the specimen thickness post texturing can at times be greater than the thickness prior to machining, which is due to the formation of pile-ups that can occur above the initial surface.

2.3. Characterization methods

2.3.1. Profile measurements

Following AWJ machining and texturing, surface topography of the target zones was measured using an InfiniteFocusSL optical surface profilometer from Alicona Corporation. The focus variation technique was utilized, capturing the coordinates of each pixel's center within the scanned area using the instruments autofocus along the optical axis. The objective lens was set at $10\times$ magnification, with vertical and lateral resolutions of 0.1 μm and 2.0 μm , respectively. Although the entire scanned area was 20×20 mm^2 , the analysis focused on the central 15×15 mm^2 region.

2.3.2. Quantification of surface quality

The surface quality of the specimens was quantified by evaluating the crater volume (Cv) formed during texturing [40]. The void areas below the mean plane are classified as 'craters.' The mean plane is established using the least squares method by the profilometer's post-processing software, a standard computational approach used to define a reference plane from the acquired surface point data. This method minimizes the sum of squared deviations between the measured points and the fitted plane, facilitating accurate representation of the surface data. In this work, data acquisition was focussed to the central 15 mm imes 15 mm region across all the specimens. Consistent measurement conditions were maintained across all trials, including the same confidence index setting of 0.9, to ensure the comparability of results across samples and conditions. Originally introduced by Hejjaji et al. [9], this approach has proven effective as a reliable method for assessing surface quality after AWJ machining of UD carbon/epoxy composites. Similarly, in the work of Sourd et al., it was shown that the critical energy release rate in Mode 1 tests on bonded 3D woven carbon/epoxy specimens correlated well with Cv, compared to other parameters such as Ra or Sa [11]. To reduce the influence of edge effects caused by the jet's entry and exit on the surface, measurements were confined to the central region [41]. Cv was then normalized by the total scanned area to enable comparison between different specimens and conditions. Additionally, the areal surface quality metric, arithmetic mean height (Sa), was obtained using Alicona software within the same measurement

2.3.3. Height quantification and characterization of defects

To assess the depth of the machined and textured specimens relative to the top surface, the specimens were imaged using a Keyence VHX-7000 digital microscope. Various magnification levels were employed with both co-axial and ring lighting. Manual adjustments included setting the shutter speed to 12.3 ms and a gain of 5 dB. For SEM analysis, a Hitachi TM 3000 scanning electron microscope was used to detect and characterize the machined and textured surfaces. Secondary electron imaging was conducted at various magnification levels to examine the nature and morphology of these surfaces. Additionally, backscattered electron (BSE) imaging was used to identify abrasive particles embedded within the textured surfaces.

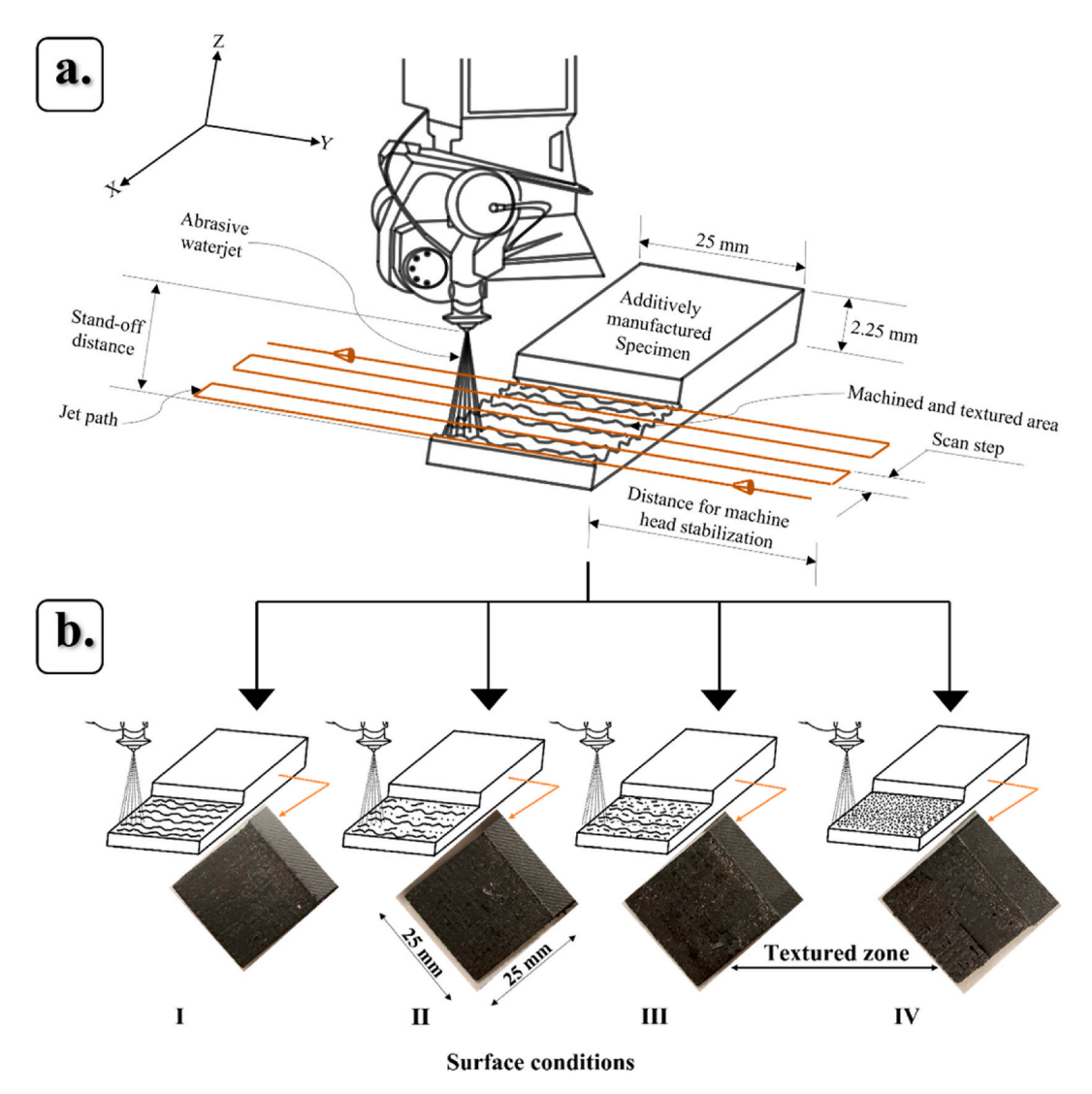


Fig. 3. Illustration of the abrasive waterjet process: a) raster scan pattern used for machining and texturing, b) Resulting surface conditions: I. machined without additional surface preparation, II. machined with light texturation (good), III. machined with moderate texturation (medium), and IV. machined with heavy texturation (poor).

 Table 4

 Description of machining and texturation conditions.

Condition	Description
I	Machined without additional surface preparation
II	Machined followed by light texturation (good)
III	Machined followed by moderate texturation (medium)
IV	Machined followed by heavy texturation (poor)

3. Results and discussion

3.1. Material removal and surface quality

The initial phase of the study focused on evaluating AWJ process parameters and texturation quality (conditions I to IV, see Fig. 3) to determine Cv, Sa, surface topographies and the mechanisms of failure. From Table 5, it can be observed that the depth (D) of material removal varies significantly between the two orientations, highlighting distinct interactions of the AWJ with respect to the fiber architectures. In the UD orientation, the depth increases steadily from 0.812 mm in condition I to 1.173 mm in condition IV, marking a 44 % rise.

This controlled increase is attributed to the uniform fiber alignment,

Table 5
Mean values of measured depths (D) of different conditions for UD and MD orientations, including nominal thickness (Tn), actual thickness (Ta) of the specimens.

Surface condition	n I		II		III		IV	
Orientation	UD	MD	UD	MD	UD	MD	UD	MD
Tn (mm)	2.3	2.5	2.3	2.5	2.3	2.5	2.3	2.5
Ta (mm)	2.37 ± 0.06	2.61 ± 0.10	2.40 ± 0.04	2.65 ± 0.09	2.39 ± 0.05	2.58 ± 0.12	2.39 ± 0.04	2.64 ± 0.11
D (mm)	0.812 ± 0.087	0.963 ± 0.058	0.893 ± 0.021	1.16 ± 0.086	0.963 ± 0.074	1.223 ± 0.093	1.173 ± 0.094	1.343 ± 0.013

which provides consistent resistance and results in predictable material removal. Conversely, in MD orientation, an initial depth begins at 0.963 mm in condition I, increasing to 1.343 mm in condition IV. While this represents a smaller percentage increase (39 %) compared to the UD case, the absolute depth values are consistently higher. These differences are due to the varied material removal mechanisms incurred during the AWJ process. Following the depth measurements, surface cartographies were analyzed to assess the effects of machining parameters on Cv, Sa, and material removal mechanisms. Fig. 4 presents the Cv and Sa values across different surface quality conditions, highlighting the correlation between surface characteristics and texturation intensity.

Cv and Sa provide a comprehensive analysis of the extent and severity of cratering. Cv offers a volumetric evaluation of crater dimensions, while Sa represents the areal 3D average roughness, capturing surface irregularities more effectively than traditional 2D line measurements like Ra [9,30]. As shown in Fig. 4, Cv and Sa values are consistently higher in MD orientation compared UD. In the MD orientation, the Cv for condition I shows a 114 % increase, while the increases in conditions II, III and IV are notably smaller at 27.42 %, 15.91 %, 8.85 % respectively. Similarly, Sa values in the MD orientation rise by 122.45 %, 128.99 %, 81.61 % and 48.22 % across conditions I to IV. These higher Cv and Sa values are attributed to the varied fiber angles in the MD orientation, which create pockets of reduced resistance, allowing deeper AWJ penetration and causing uneven material removal. The results are further analyzed through surface topography and SEM characterization.

Fig. 5 illustrates the variation in surface topographies for both orientations. The intensity of surface texture progressively increases from condition I to IV in both UD and MD orientations. In AWJ machining, high-velocity abrasive particles strike the material surface with substantial kinetic energy, which is converted into mechanical energy upon impact [42]. This energy transfer results in localized micro-fracture erosion in the matrix and fibers, leading to material removal in the form of craters. The fracturing of the matrix and carbon fibers is a primary mechanism of material removal [9]. As the kinetic energy from the abrasive particles surpasses the fracture toughness of the material, microcracks form, propagate, and eventually cause fibers to break apart while the softer matrix undergoes plastic deformation and erosion [26]. As the dominant influential input parameters - waterjet pressure and jet traverse speed - increase, the frequency and force of particle impact increase, intensifying material removal [8]. The increase in impact energy accelerates the microfracture process, resulting in deeper craters and more pronounced erosion [9]. While both orientations exhibit similar material removal patterns, notable differences are evident in the

extent of surface damage.

The primary features identified are cratering, matrix erosion, and pile-up defects, all caused by abrasive impacts during the AWJ process [43,44]. Cratering occurs when high velocity abrasive particles strike the surface, leading to localized erosion and material displacement [19]. Matrix erosion describes the gradual recession and removal of the matrix material, while pile-up defects emerge when displaced material accumulates near trenches and crater edges due to incomplete material removal [45]. As AWJ input variables intensify, material removal increases, leading to increased dislodgement [46,47]. However, some dislodged material may remain, causing pile-up and result in uneven surface topography. This effect is especially prominent in MD composites, where the jet impacts fibers at varying angles, creating localized resistance that hinder complete material removal. The increasing severity of surface damage from condition I to IV is evident in the SEM analysis (Figs. 6 and 7), which offer detailed insights into fiber-matrix interactions and material degradation. The SEM images capture the progressive damage in both the matrix and fibers, showing evidence of fiber breakage, matrix peeling, and erosion. These images correlate with the rising Cv and Sa values presented in Fig. 4, reinforcing the link between surface topography and the degree of material removal.

In the UD orientation, as shown in Fig. 6a, the jet encounters significant resistance at the fiber-matrix interface, which results in shallow and consistent material removal, primarily affecting the matrix surrounding the fibers. The material removal is driven by the abrasive impact of the jet. Due to the low porosity in UD orientation, uniform material removal can be expected as the jet erodes the matrix material surrounding the fibers. In this condition, minimal fiber breakage occurs, as the jet does not have enough force to fully penetrate and dislodge the fibers. Instead, matrix peel-off is the dominant material removal mechanism, where the surrounding matrix material is eroded due to the jet's impact. This controlled removal leads to lower Cv (1.343 mm³/cm²) and Sa (41.40 µm) values, as observed in comparison to other conditions. Similar studies have been carried out by Hejjaji et al. for the case of carbon/epoxy composites [9].

As texturing begins on a surface that has already been machined (condition II - P=80 MPa, TS=10 m/min), the depth increases to 0.893 mm as the jet continues to erode the pre-machined matrix more aggressively. The material removal deepens but remains controlled, with fibers limiting further jet penetration. Initial fiber debonding, pronounced matrix peel-off, and abrasive embedment can be observed. The fiber debonding indicates that the jet has begun to overcome fiber resistance, exceeding the interfacial strength between the fibers and matrix, resulting in deeper cratering and increased surface irregularities

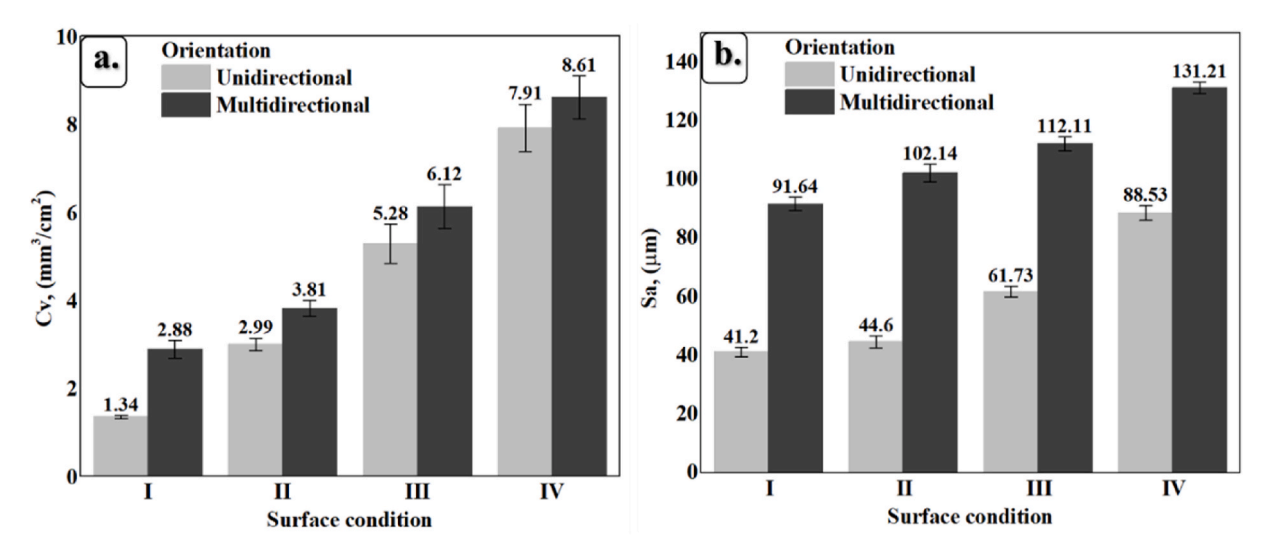


Fig. 4. Cv and Sa values across surface conditions I to IV for both UD and MD orientations.

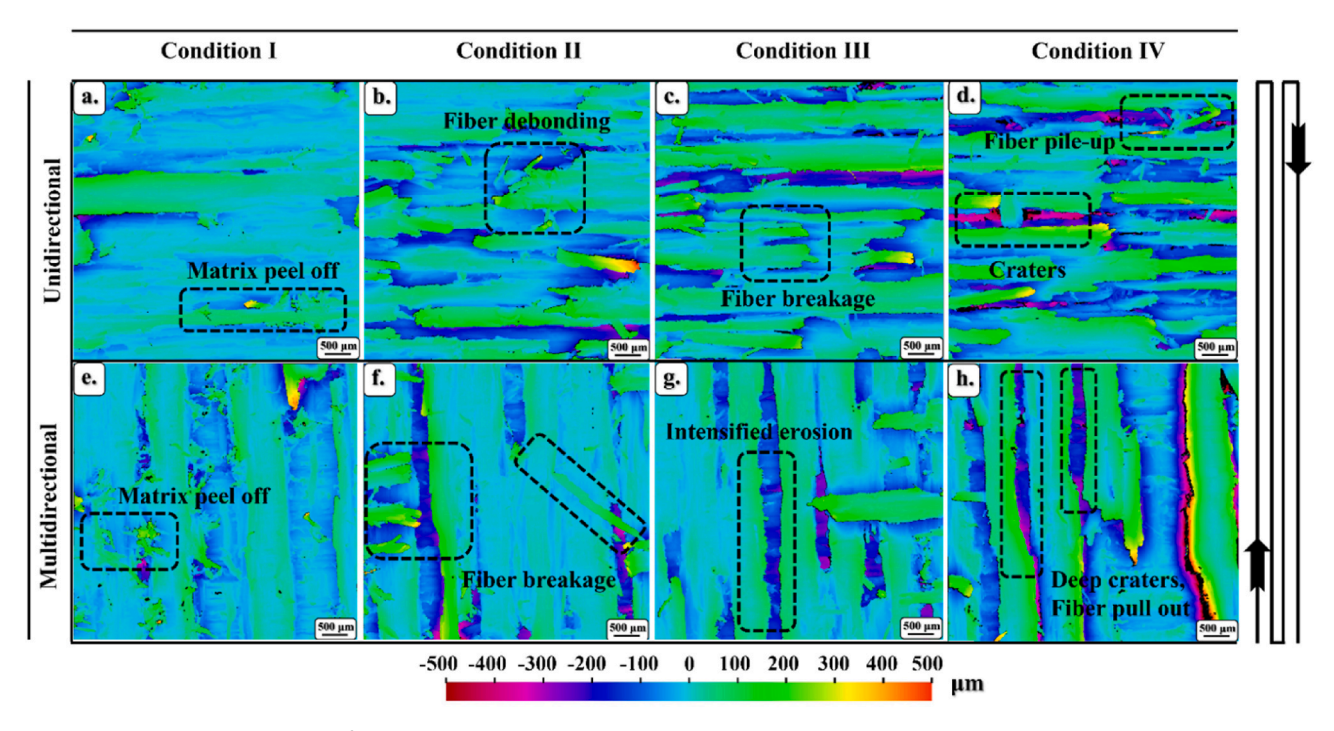


Fig. 5. Surface topographies (15 × 15 mm²) for UD (a-d) and MD (e-h) orientations across surface conditions I to IV, the direction of waterjet is also indicated.

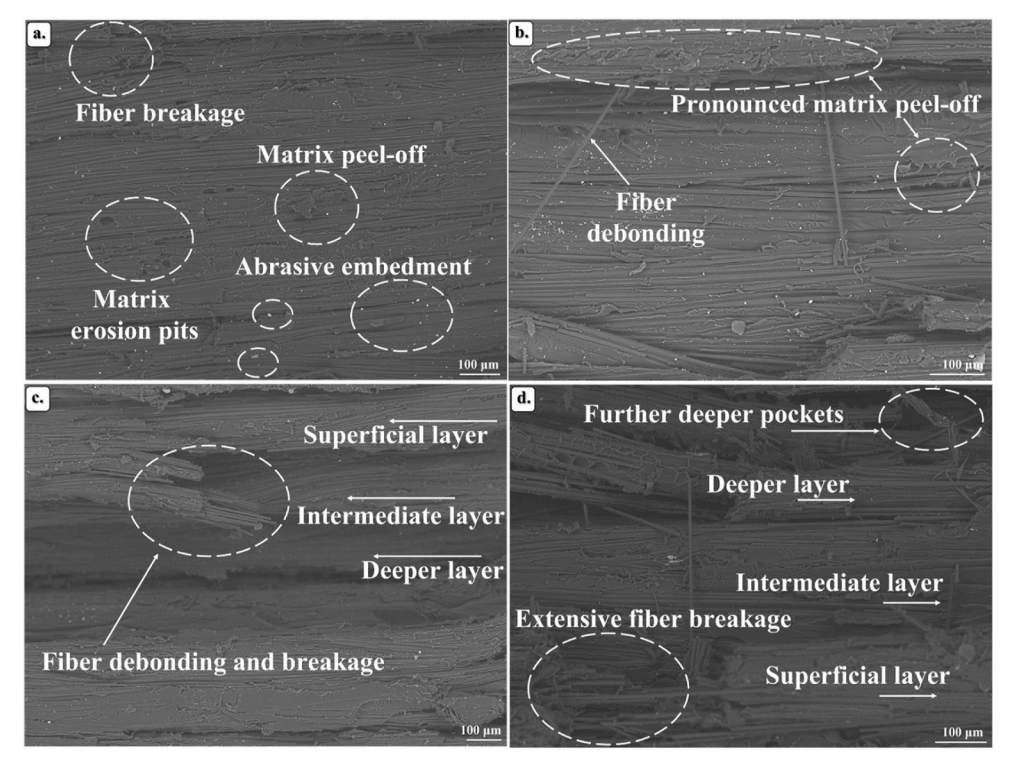


Fig. 6. SEM micrographs of UD composites under different conditions: (a) condition I, (b) condition II, (c) condition III, and (d) condition IV.

as shown in Fig. 6b. By further texturing (condition III - P = 85 MPa, TS = 10 m/min), the depth reaches 0.963 mm as the fiber-matrix bond weakens. The increased pressure delivers higher kinetic energy to the abrasive particles, intensifying erosion and shear forces at the fiber matrix boundary. These forces exceed the interfacial strength causing debonding and breakage as fibers begin to separate from the matrix (Fig. 6c). The higher Cv (5.28 mm³/cm²) and Sa (61.73 μ m) values reflect the formation of more pronounced craters and increased surface

roughness. The jet's impact not only removes material but also leads to pile-up of fibers and matrix debris, causing uneven surface topography. During heavy texturation (condition IV - P = 100 MPa, TS = 15 m/min), the depth increases to 1.173 mm as the high-pressure jet cuts into the fibers and extensively erodes the matrix. The increased energy allows the abrasive particles to penetrate the matrix and fibers, despite the perpendicular fiber alignment, which limits deeper penetration. Extensive fiber breakage, deep matrix pockets, and significant matrix erosion

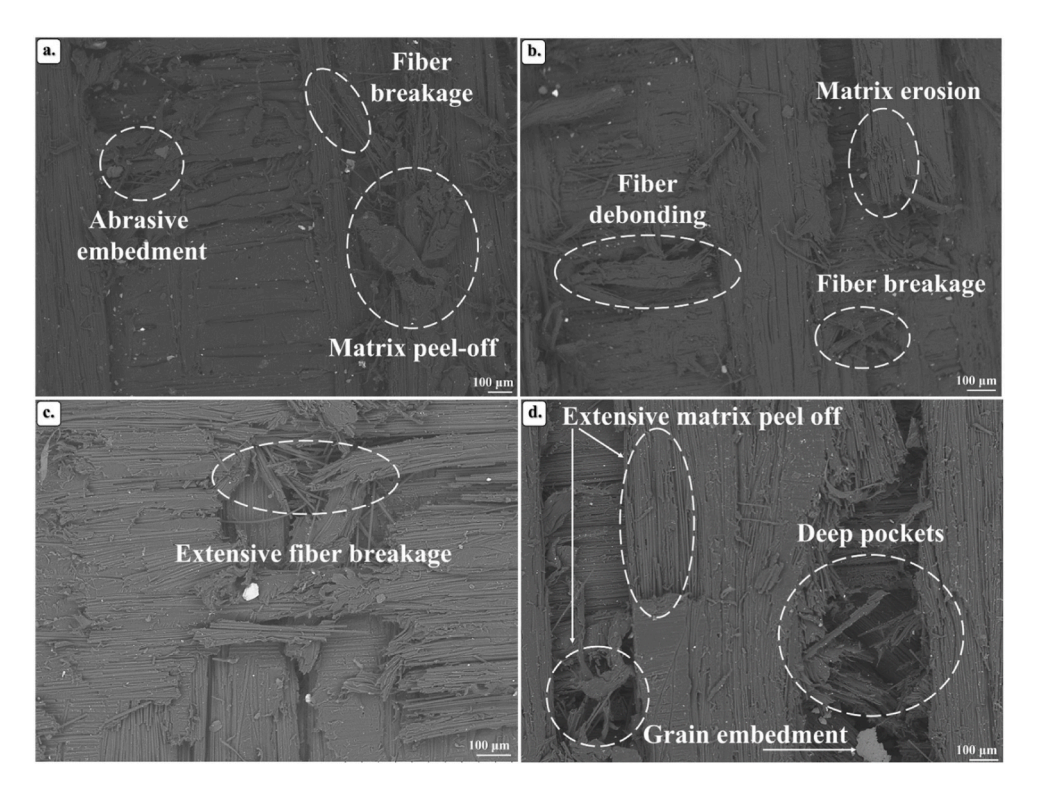


Fig. 7. SEM micrographs of MD composites under different conditions: (a) condition I, (b) condition II, (c) condition III, and (d) condition IV.

are observed (Fig. 6d), along with pile-up damage from fiber dislodgement and matrix recession. The highest Cv (7.906 $\rm mm^3/cm^2)$ and Sa (88.55 $\mu m)$ values reflect the severe damage observed in this condition. Therefore, in the UD orientation, where fibers are perpendicular to the jet, shear forces generated by the jet act majorly along the fiber-matrix interface. The jet faces consistent fiber resistance, making it challenging to fully cut through the fibers, resulting in incomplete fiber breakage, causing irregularities such as pile-up, as the matrix is removed more easily than the fibers.

In MD orientation, the AWJ encounters more complex interactions due to higher porosity, or matrix rich zones, allowing the jet to exploit weaker points where fibers are oriented obliquely or parallel to the jet. In condition I (P = 100 MPa, TS = 5 m/min), the initial depth is 0.963mm – higher than that of the UD orientation. This can be attributed to the variation in shear forces along the fiber-matrix boundaries. When the jet interacts with fibers at non-perpendicular angles, localized stresses exceed the fiber-matrix interfacial strength, leading to matrix peel-off and initial fiber breakage. The lower interfacial shear strength in these regions allows the high-velocity particles to penetrate more deeply, forming larger craters compared to the UD case. The increase in Sa results from the uneven removal of fibers and matrix, as, the MD orientations lead to local mechanical failures when the jet's impact forces exceed the critical strength of fibers. Matrix peel-off, initial fiber breakage, and abrasive embedment are prevalent, as observed in Fig. 7a. The higher initial Cv (2.873 mm 3 /cm 2) and Sa (91.64 μ m) values reflect this behavior. In condition II (P = 80 MPa, TS = 10 m/min), the texturing process builds on the previously machined surface, further increasing the depth to 1.16 mm. The fibers, already weakened by the initial machining, undergo further degradation as the jet penetrates the now rougher surface. Extensive fiber debonding, matrix erosion, and fiber breakage are evident due to additional damage and fiber-matrix separation (Fig. 7b). This leads to an increased Cv (3.986 mm³/cm²) and Sa (102.14 µm) values, reflecting deeper cratering and rougher surface texture. In condition III (P = 85 MPa, TS = 10 m/min), the increased input pressure leads to further depth increase and intensified erosion. The abrasive particles gain more kinetic energy, resulting in

higher impact forces upon striking the surface. The additional energy is sufficient to overcome the bonding forces at the fiber-matrix interface causing localized degradation. Extensive fiber breakage, matrix degradation, and deep cratering as observed in Fig. 7c. The higher Cv (6.113 mm³/cm²) and Sa (112.10 μm) values align with the severe material removal and uneven surface damage. During heavy texturation (condition IV, P = 100 MPa, TS = 15 m/min), an increase in depth further to 1.343 mm is observed. The high jet pressure drives aggressive mechanical erosion resulting in substantial material removal characterized by deep craters, significant fiber pullouts and pile-up (Fig. 7d). The highest Cv (8.61 mm³/cm²) and Sa (131.21 μm) values are consistent with the severity of the observed damage. In MD orientation, the fiber alignment at various angles allows the jet to penetrate more deeply in localized areas. The shear forces exerted by the AWJ vary significantly across the surface depending on the fiber orientation. When the jet interacts with fibers at angles other than perpendicular, it more effectively acts along the fiber-matrix interface, leading to easier separation or cutting of fibers. Overall, the MD orientation exhibits more substantial and erratic material removal across all conditions, driven by the complex and non-uniform resistance due to varied fiber orientations, in contrast to the more predictable and controlled behavior observed in the UD orientation.

3.2. Predictive modeling for Cv and Sa

Predictive models were developed to quantify critical machining outcomes, specifically the Cv and Sa, for both UD and MD composite materials. The machining parameters considered – waterjet pressure (P), traverse speed (TS), and scan step (SS) – were chosen based on their established significance in previous research as the most influential factors in AWJ [9]. Data from these experiments informed the development of predictive models using power-law relationships, following a modeling approach similar to that used in earlier research by Sourd et al. [4], which has proven effective in similar machining context for 3D woven carbon/epoxy materials. A power – law relationship is a mathematical representation to model that describes how a dependent

variable is influenced by independent variables, each raised to a specific power. In our work, this relationship is used to model the influence of machining parameters on surface quality metrics. The dependent variables in this context are Cv and Sa, and the independent variables are P, TS, and SS. Each independent variable is raised to a specific power, representing the sensitivity of the dependent variable to changes in the independent variables (equations (2) and (3)). Non-linear regression techniques were employed to fit the experimental data to the chosen model forms, with coefficients optimized to minimize prediction error. The models were validated using a subset of data not included in the initial fitting, ensuring their predictive accuracy. Percentage differences between predicted and experimental values were analyzed to evaluate the models' precision, and where discrepancies were identified, the models were iteratively refined by adjusting the coefficients. Separate predictive models were developed for Sa and Cv for both UD and MD, denoted as Sa_{uni}, Sa_{multi}, Cv_{uni}, and Cv_{multi}. These models take the general form:

$$Sa = a \cdot P^b \cdot TS^c \cdot SS^d$$
 (2)

$$Cv = a \cdot P^b \cdot TS^c \cdot SS^d$$
 (3)

In equations (2) and (3), the constants a, b, c, and d represent interpolation coefficients that depend on the material properties and the specific set of machining conditions. To determine these coefficients, 90 % of the experimental data was utilized to train the model, while the remaining 10 % was reserved for model validation. After the identification process, the calculated constants are presented in Eqs. (4)–(7).

$$Sa_{uni} = 0.0301 \cdot P^{1.3350} \cdot TS^{0.6816}$$
 (4)

$$Sa_{multi} = 7.4291 \cdot P^{0.4312} \cdot TS^{0.3305}$$
 (5)

$$Cv_{uni} = 0.0105 \cdot P^{0.5946} \cdot TS^{1.4412}$$
 (6)

$$Cv_{multi} = 0.0051 \cdot P^{1.0556} \cdot TS^{0.9541}$$
 (7)

In these equations, P represents waterjet pressure in MPa, TS represents jet traverse speed in m/min, and SS represents scan step in mm (fixed at 1 mm in this study). The coefficients a, b, and c were determined through regression analysis, capturing the material's machinability and the sensitivity of the outcomes to these respective parameters. Although SS was held constant in this experimental campaign, an exponent 'd' for SS would account for its influence if varied. The predictive models for both Cv and Sa demonstrate good accuracy for both orientations, as indicated by the R² values obtained. For Cv, the model achieves a correlation factor of 0.87 for UD and 0.84 for MD composite (Fig. 8a and b), effectively capturing major variances in crater volume, despite complexities of modeling material removal at the micro-level due to combined interactions of variables. Similarly, the model for Sa exhibits even higher predictive accuracy, with values of R² at 0.9 and 0.92 for UD and MD orientations, respectively (Fig. 8c and d). These slightly higher values of Sa indicate a closer agreement with experimental results in comparison with Cv. In UD case, Sa is more uniform and predictable due to the consistent fiber alignment.

The validation between predicted and experimental values is presented in Table 6. The degree of validity of the model predictions was evaluated by comparing these predicted and experimental values of Sa and Cv. The relative errors for Cv were 11.71 % and 6.85 % for UD and MD specimens, respectively. For Sa, the relative errors were 3.3 % for UD and 2.61 % for MD orientations. Although the models generally perform well, certain parameters – such as the intricate interactions between fiber and matrix, localized variations in jet dispersion and specific energy transfer during machining – are inherently complex and challenging to fully incorporate into the existing modeling framework.

These complexities contribute to the residual variations between the predicted and measured outcomes, affecting the R^2 values relative to unity. Additionally, in this experimental campaign, the texturation

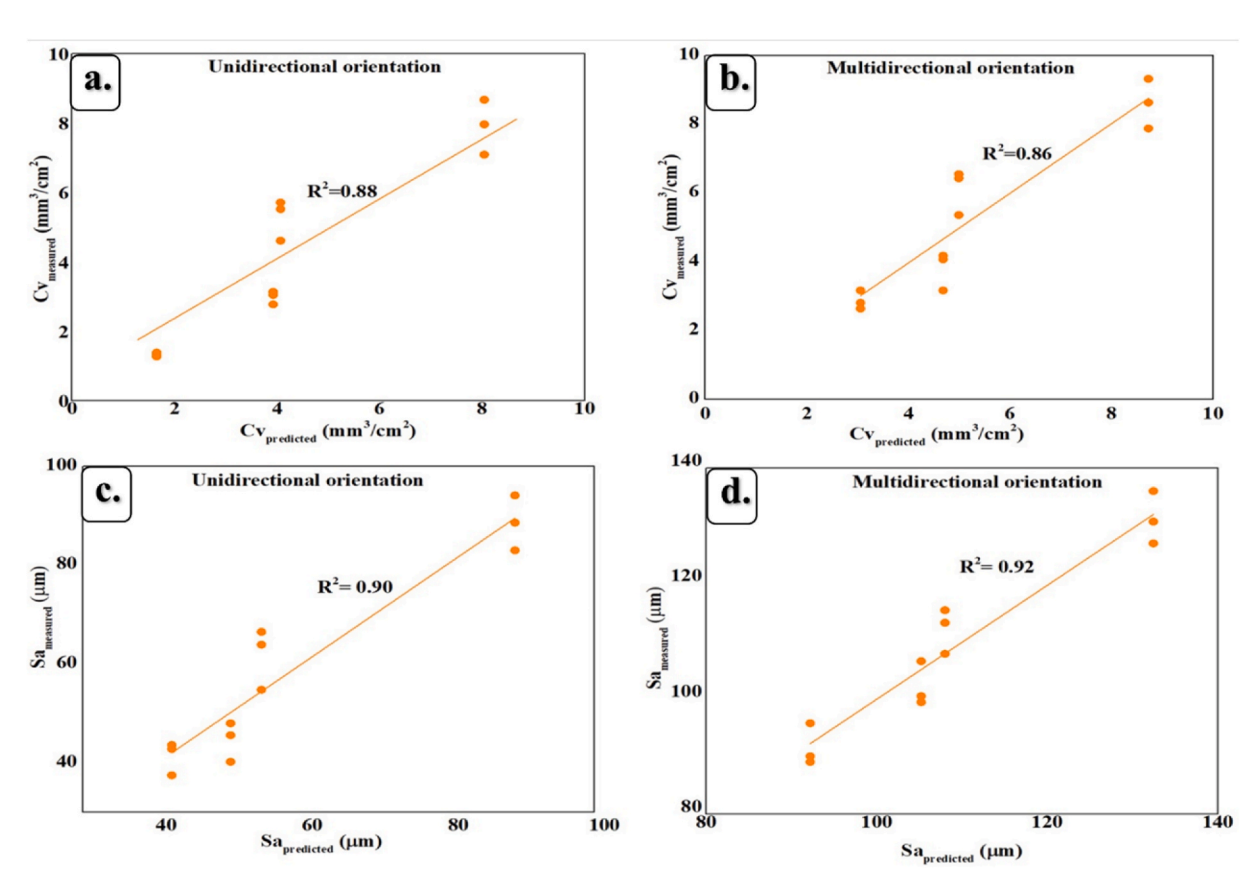


Fig. 8. Results of the prediction model of Cv and Sa showing predicted values with respect to experimental ones for UD and MD orientations.

Table 6
Validation of the predictive model by comparing experimental and predicted values for Cv and Sa in UD and MD orientations.

Orientation	Sa (µm)	Sa (μm)			$Cv (mm^3/cm^2)$		
	Condition	Experimental	Predicted	Condition	Experimental	Predicted	
Uni	I	43.6	42.16	II	4.61	4.0702	
Multi	IV	135.99	132.44	III	5.36	4.993	

process was applied to surfaces that had already undergone machining. This sequential approach means that the surface characteristics formed during machining served as a foundation for subsequent texturing. In consequence, the final Cv and Sa values are influenced not only by the texturing parameters, but also the pre-existing conditions from machining. This combined effect introduces additional variability that may be difficult to account for in the predictive model. Surface irregularities, residual stresses and micro-level deformations from the initial machining could accumulate on the textured surfaces, potentially leading to deviations from the predicted outcomes.

4. Conclusions

This study explored the use of AWJ process for controlled depth machining and surface texturation of MEX fabricated composite materials, with a focus on identifying critical input parameters like waterjet pressure and traverse speed. The following key conclusions are drawn.

- Cv and Sa values showed a consistent increase from condition I to IV in both UD and MD orientations, highlighting the effectiveness of the AWJ process achieving desired surface characteristics. In the UD orientation, Cv rose from 1.34 mm³/cm² to 7.91 mm³/cm², and Sa from 41.2 μm to 88.53 μm. For MD, Cv increased from 2.88 mm³/cm² to 8.61 mm³/cm², while Sa rose from 91.64 μm to 131.21 μm.
- Surface topographical analysis showed a clear progression of irregularities and texture variations from condition I to IV. In condition I, matrix peel-off was observed in both UD and MD orientations. However, by condition IV, the features diverged: UD composites demonstrated debonding and significant fiber breakage, while MD composites showed deeper craters and extensive fiber pull-out. This difference in condition IV is attributed to the varied fiber orientations of MD composites, creating pockets of lower resistance, allowing deeper AWJ penetration and uneven material removal.
- SEM characterization revealed variations in crater formation and fiber-matrix interactions across surface conditions I to IV, supporting the observations from the topographical analysis.
- Predictive models for Cv and Sa were developed and validated, showing strong agreement with experimental results. The R² values for Cv and Sa were 0.88 and 0.90 for UD, and 0.86 and 0.92 for MD, indicating good alignment between the model predictions and experimental data.

This research highlights the effectiveness of AWJ machining and texturation in developing varied surface characteristics of MEX fabricated composite materials, offering valuable insights for advancing precision in high-performance applications such as aerospace engineering.

Declaration of competing interest

The authors declare that they have no known competing financial interests or personal relationships that could have appeared to influence the work reported in this paper.

Acknowledgements

The authors express their gratitude for the financial support provided

by the Réseau de Recherche en Économie Circulaire du Québec (RRECQ), as well as the funding received from École de technologie supérieure's CIR grant aimed at fostering international research collaborations. We also extend our thanks to the MITACS research organization for awarding the Globalink International Research Award (IT34850). Additionally, we acknowledge the financial assistance from the Natural Sciences and Engineering Research Council of Canada (NSERC) through the Discovery Grant (RGPIN-2019-05973).

References

- S.A. Delbari, L.A. Hof, Glass waste circular economy advancing to high-value glass sheets recovery using industry 4.0 and 5.0 technologies, J. Clean. Prod. 462 (2024) 142629, https://doi.org/10.1016/j.jclepro.2024.142629.
- [2] C. Mejía-Moncayo, J.-P. Kenné, L.A. Hof, On the development of a smart architecture for a sustainable manufacturing-remanufacturing system: a literature review approach, Comput. Ind. Eng. 180 (2023) 109282, https://doi.org/10.1016/ i.cie.2023.109282.
- [3] V. Delpla, J.-P. Kenné, L.A. Hof, Circular manufacturing 4.0: towards internet of things embedded closed-loop supply chains, Int. J. Adv. Manuf. Technol. 118 (2022) 3241–3264, https://doi.org/10.1007/s00170-021-08058-3.
- [4] X. Sourd, R. Zitoune, L. Crouzeix, M. Salem, M. Charlas, New model for the prediction of the machining depth during milling of 3D woven composite using abrasive waterjet process, Compos. Struct. 234 (2020) 111760, https://doi.org/ 10.1016/j.compstruct.2019.111760.
- [5] G. Prashar, H. Vasudev, D. Bhuddhi, Additive manufacturing: expanding 3D printing horizon in industry 4.0, Int. J. Interact. Des. Manuf. 17 (2023) 2221–2235, https://doi.org/10.1007/s12008-022-00956-4.
- [6] A. Chandra Shekar, A. Hadj Djilani, R. Zitoune, L. Toubal, L.A. Hof, Effect of input variables on the mechanical properties of additively manufactured PEEK thermoplastics, Mater. Today Proc. (2023), https://doi.org/10.1016/j. matpr.2023.09.101.
- [7] S. Kuschmitz, A. Schirp, J. Busse, H. Watschke, C. Schirp, T. Vietor, Development and processing of continuous flax and carbon fiber-reinforced thermoplastic composites by a modified material extrusion process, Materials 14 (2021) 2332, https://doi.org/10.3390/ma14092332.
- [8] A. Hejjaji, R. Zitoune, L. Crouzeix, S.L. Roux, F. Collombet, Surface and machining induced damage characterization of abrasive water jet milled carbon/epoxy composite specimens and their impact on tensile behavior, Wear 376–377 (2017) 1356–1364, https://doi.org/10.1016/j.wear.2017.02.024.
- [9] A. Hejjaji, R. Zitoune, L. Toubal, L. Crouzeix, F. Collombet, Influence of controlled depth abrasive water jet milling on the fatigue behavior of carbon/epoxy composites, Compos. Appl. Sci. Manuf. 121 (2019) 397–410, https://doi.org/ 10.1016/j.compositesa.2019.03.045.
- [10] X. Sourd, R. Zitoune, A. Hejjaji, M. Salem, L. Crouzeix, D. Lamouche, Multi-scale analysis of the generated damage when machining pockets of 3D woven composite for repair applications using abrasive water jet process: contamination analysis, Compos. Appl. Sci. Manuf. 139 (2020) 106118, https://doi.org/10.1016/j. compositesa.2020.106118.
- [11] X. Sourd, R. Zitoune, L. Crouzeix, M. Coulaud, Influence of the texturing quality consecutive to Abrasive Water Jet machining on the adhesive properties in mode I of 3D woven composite assemblies, Compos. B Eng. 242 (2022) 110091, https:// doi.org/10.1016/j.compositesb.2022.110091.
- [12] M. Haddad, R. Zitoune, F. Eyma, B. Castanie, Study of the surface defects and dust generated during trimming of CFRP: influence of tool geometry, machining parameters and cutting speed range, Compos. Appl. Sci. Manuf. 66 (2014) 142–154, https://doi.org/10.1016/j.compositesa.2014.07.005.
- [13] N. Nguyen-Dinh, R. Zitoune, C. Bouvet, S. Leroux, Surface integrity while trimming of composite structures: X-ray tomography analysis, Compos. Struct. 210 (2019) 735–746. https://doi.org/10.1016/i.compstruct.2018.12.006.
- [14] R. Teti, Machining of composite materials, CIRP Annals 51 (2002) 611–634, https://doi.org/10.1016/S0007-8506(07)61703-X.
- [15] N. Nguyen-Dinh, A. Hejjaji, R. Zitoune, C. Bouvet, M. Salem, New tool for reduction of harmful particulate dispersion and to improve machining quality when trimming carbon/epoxy composites, Compos. Appl. Sci. Manuf. 131 (2020) 105806, https://doi.org/10.1016/j.compositesa.2020.105806.
- [16] M. Ramulu, D. Arola, The influence of abrasive waterjet cutting conditions on the surface quality of graphite/epoxy laminates, Int. J. Mach. Tool Manufact. 34 (1994) 295–313, https://doi.org/10.1016/0890-6955(94)90001-9.
- [17] D. Arola, M. Ramulu, Net shape manufacturing and the performance of polymer composites under dynamic loads, Exp. Mech. 37 (1997) 379–385, https://doi.org/ 10.1007/BF02317300.

- [18] M. Haddad, R. Zitoune, F. Eyma, B. Castanié, Influence of machining process and machining induced surface roughness on mechanical properties of continuous fiber composites, Exp. Mech. 55 (2015) 519–528, https://doi.org/10.1007/s11340-014-9967.x
- [19] X. Sourd, R. Zitoune, A. Hejjaji, M. Salem, A. Hor, D. Lamouche, Plain water jet cleaning of titanium alloy after abrasive water jet milling: surface contamination and quality analysis in the context of maintenance, Wear 477 (2021) 203833, https://doi.org/10.1016/j.wear.2021.203833.
- [20] M. Hashish, Abrasive waterjet machining, Materials 17 (2024) 3273, https://doi. org/10.3390/ma17133273.
- [21] M. Monoranu, S. Ashworth, R. M'Saoubi, J.P. Fairclough, K. Kerrigan, R.J. Scaife, S. Barnes, H. Ghadbeigi, A comparative study of the effects of milling and abrasive water jet cutting on flexural performance of CFRP, Procedia CIRP 85 (2019) 277–283, https://doi.org/10.1016/j.procir.2019.09.036.
- [22] S. Akıncıoğlı, Investigation of effect of abrasive water jet (AWJ) machining parameters on aramid fiber-reinforced polymer (AFRP) composite materials, Aircraft Eng. Aero. Technol. 93 (2021) 615–628, https://doi.org/10.1108/AEAT-11.2020.0249
- [23] M. Haddad, R. Zitoune, H. Bougherara, F. Eyma, B. Castanié, Study of trimming damages of CFRP structures in function of the machining processes and their impact on the mechanical behavior, Compos. B Eng. 57 (2014) 136–143, https:// doi.org/10.1016/j.compositesb.2013.09.051.
- [24] A.W. Momber, R. Kovacevic, Material-removal mechanisms in abrasive water-jet machining, in: A.W. Momber, R. Kovacevic (Eds.), Principles of Abrasive Water Jet Machining, Springer, London, 1998, pp. 89–162, https://doi.org/10.1007/978-1-4471.1579-4
- [25] M. Ramulu, D. Arola, Water jet and abrasive water jet cutting of unidirectional graphite/epoxy composite, Composites 24 (1993) 299–308, https://doi.org/ 10.1016/0010-4361(93)90040-F.
- [26] D. Arola, M. Ramulu, A study of kerf characteristics in abrasive waterjet machining of graphite/epoxy composite, J. Eng. Mater. Technol. 118 (1996) 256–265, https://doi.org/10.1115/1.2804897.
- [27] P. Ghidossi, M. El Mansori, F. Pierron, Edge machining effects on the failure of polymer matrix composite coupons, Compos. Appl. Sci. Manuf. 35 (2004) 989–999, https://doi.org/10.1016/j.compositesa.2004.01.015.
- [28] C.A. Squires, K.H. Netting, A.R. Chambers, Understanding the factors affecting the compressive testing of unidirectional carbon fibre composites, Compos. B Eng. 38 (2007) 481–487, https://doi.org/10.1016/j.compositesb.2006.08.002.
- [29] M. Ramulu, K. Colligan, Edge Finishing and Delamination Effects Induced During Abrasive Waterjet Machining on the Compression Strength of a Graphite/Epoxy Composite, in: n.d. https://doi.org/10.1115/IMECE2005-82346.
- [30] S. Pourrahimi, L.A. Hof, On the Post-Processing of Complex Additive Manufactured Metallic Parts: A Review, Advanced Engineering Materials n/a (n.d.) 2301511. https://doi.org/10.1002/adem.202301511.
- [31] N. Nguyen-Dinh, C. Bouvet, R. Zitoune, Influence of machining damage generated during trimming of CFRP composite on the compressive strength, J. Compos. Mater. 54 (2020) 1413–1430, https://doi.org/10.1177/0021998319883335.
- [32] Onyx Composite 3D Printing Material, (n.d.). https://markforged.com/materials/plastics/onyx (accessed June 18, 2024).
- [33] composites-data-sheet.pdf, (n.d.). https://static.markforged.com/downloads/com posites-data-sheet.pdf (accessed March 9, 2024).

- [34] T. Dong, N.H. Kim, Cost-effectiveness of structural health monitoring in fuselage maintenance of the civil aviation industry †, Aerospace 5 (2018) 87, https://doi. org/10.3390/aerospace5030087.
- [35] D. Roach, Real Time Crack Detection Using Mountable Comparative Vacuum Monitoring Sensors, 1 5, 2009, pp. 317–328.
- [36] M. Van Tooren, L. Krakers, Multi-disciplinary design of aircraft fuselage structures, in: 45th AIAA Aerospace Sciences Meeting and Exhibit, American Institute of Aeronautics and Astronautics, Reno, Nevada, 2007, https://doi.org/10.2514/ 6.2007-767
- [37] F. Ghebretinsae, O. Mikkelsen, A.D. Akessa, Strength analysis of 3D printed carbon fibre reinforced thermoplastic using experimental and numerical methods, IOP Conf. Ser. Mater. Sci. Eng. 700 (2019) 012024, https://doi.org/10.1088/1757-899X/700/1/012024.
- [38] P. Fréquelin, R. Zitoune, J. Jumel, S. Le Roux, A. Jaillon, F. Cénac, A semianalytical model for low-density impact-based surface treatments: application to the abrasive waterjet texturing of thermoplastic polymers, Tribol. Int. 201 (2025) 110256, https://doi.org/10.1016/j.triboint.2024.110256.
- [39] A.C. Shekar, A. Sawalmeh, R. Zitoune, L.A. Hof, Optimization of surface texturing parameters in additively manufactured continuous fiber composites using abrasive waterjet technique for composite repair applications, Compos. Appl. Sci. Manuf. 190 (2025) 108698, https://doi.org/10.1016/j.compositesa.2024.108698.
- [40] X. Sourd, R. Zitoune, L. Crouzeix, M. Coulaud, Influence of the texturing quality consecutive to Abrasive Water Jet machining on the adhesive properties in mode I of 3D woven composite assemblies, Compos. B Eng. 242 (2022) 110091, https:// doi.org/10.1016/j.compositesb.2022.110091.
- [41] L.C. Salinas, K. Moussaoui, A. Hejjaji, M. Salem, A. Hor, R. Zitoune, Influence of abrasive water jet parameters on the surface integrity of Inconel 718, Int. J. Adv. Manuf. Technol. 114 (2021) 997–1009, https://doi.org/10.1007/s00170-021-06888-0
- [42] Y. Ozcan, L.T. Tunc, J. Kopacka, B. Cetin, M. Sulitka, Modelling and simulation of controlled depth abrasive water jet machining (AWJM) for roughing passes of freeform surfaces, Int. J. Adv. Manuf. Technol. 114 (2021) 3581–3596, https://doi. org/10.1007/s00170-021-07131-1.
- [43] Z. Říha, M. Zeleňák, T. Kruml, J. Poloprudský, Comparison of the disintegration abilities of modulated and continuous water jets, Wear 478–479 (2021) 203891, https://doi.org/10.1016/j.wear.2021.203891.
- [44] J. Schwartzentruber, J.K. Spelt, M. Papini, Prediction of surface roughness in abrasive waterjet trimming of fiber reinforced polymer composites, Int. J. Mach. Tool Manufact. 122 (2017) 1–17, https://doi.org/10.1016/j. iimachtools.2017.05.007.
- [45] M. Mieszala, P.L. Torrubia, D.A. Axinte, J.J. Schwiedrzik, Y. Guo, S. Mischler, J. Michler, L. Philippe, Erosion mechanisms during abrasive waterjet machining: model microstructures and single particle experiments, J. Mater. Process. Technol. 247 (2017) 92–102, https://doi.org/10.1016/j.jmatprotec.2017.04.003.
- [46] S. Bhowmik, A. Ray Jagadish, Abrasive water jet machining of composite materials, in: K. Gupta (Ed.), Advanced Manufacturing Technologies: Modern Machining, Advanced Joining, Sustainable Manufacturing, Springer International Publishing, Cham, 2017, pp. 77–97, https://doi.org/10.1007/978-3-319-56099-1
- [47] M.A. Doğan, L. Gemi, Ş. Yazman, F. Ceritbinmez, A. Yapici, Effect of hybridization and stacking sequence on damage development in AWJ machining of Al/FRP/Al FML composites, J. Manuf. Process. 131 (2024) 141–159, https://doi.org/ 10.1016/j.jmapro.2024.09.017.